Coherent exchange and double beam splitter oscillations in a triple quantum dot

G. C. Aers, S. A. Studenikin, G. Granger, A. Kam, P. Zawadzki, Z. R. Wasilewski, and A. S. Sachrajda*
National Research Council Canada, Ottawa, Ontario, Canada K1A 0R6
(Received 4 May 2012; published 18 July 2012)

Recent experiments with an electrostatically gated structure demonstrated coherent oscillations, involving all three spins of a linear triple dot system. In a combined experimental and theoretical study, we demonstrate coherent doublet/doublet exchange oscillations, leading to arbitrary rotation on the relevant Bloch sphere, and we reveal an interplay between exchange and hyperfine-driven "double coherent beam splitter" oscillations.

DOI: 10.1103/PhysRevB.86.045316 PACS number(s): 73.63.Kv, 73.23.−b

The potential applications of a triple quantum dot system have been outlined in many theoretical papers over the past decade,[1–5] and linear triple dot devices have now been demonstrated experimentally.[6–9] The relevant location within the triple dot stability diagram for spin qubits is the connected (2,0,1), (1,1,1) and (1,0,2) regime where the (2,0,1) and (1,0,2) regions are required for spin-to-charge conversion. Crossing this space [Fig. 1(c)], the exchange coupling between the center spin and one edge spin decreases while simultaneously increasing with the other. This results in two levels, $\Delta'_{1/2}$ and $Q_{3/2}$, anticrossing twice (due to hyperfine interactions). In a recent paper,[10] we demonstrated coherent Landau-Zener-Stuckelberg (LZS) oscillations between these two three-spin levels utilizing each anticrossing as a "beam splitter" for quantum state preparation in a similar way to that utilized in double quantum dots.[11] In this paper, we analyze, theoretically and experimentally, the coherent behavior obtained for a pulse through "both" anticrossings and find an interplay between hyperfine-driven double beam splitter oscillations and pure exchange oscillations of the triple dot system (made clear by varying both pulse detuning and magnetic field). The latter oscillations are proposed for an exchange-only architecture by DiVincenzo *et al.*[1] where quantum information is encoded in triple quantum dot states in a way which allows all necessary quantum computing operations to be achieved by local electrostatic gate operations. By comparison with theory, we show that this triple quantum dot qubit displays the appropriate coherent behavior associated with universal state rotation around the Bloch sphere.[9]

The linear triple dot device[6,7,10] is shown in Fig. 1(a). Charge detection measurements can be performed with either of the quantum point contacts[12] (QPCs) on each side of the device. The charge state of the device is controlled using gates 1 and 2 in combination to manipulate the tunneling between the central dot and its neighbors as well as the chemical potentials of the dots. Gate C primarily tunes the (1,1,1) charge region width.

A typical charge detection stability diagram obtained under dc conditions is shown in Fig. 1(b). In this paper, we study the coherent spin response in a spin qubit regime from the $(N_L, N_C, N_R) = (2,0,1)$ through the (1,1,1) to near the (1,0,2) electronic charge configuration, where L, C, and R refer to the left, center, and right quantum dots, respectively. The charge-transfer lines between the left and center dots (indicated by the white arrow and denoted here as ϵ_-), and the right and center dots (indicated by the blue arrow and denoted here as ϵ_+) are seen as yellow lines. The white dashed line in Fig. 1(b) illustrates a typical pulse detuning line ϵ across the (1,1,1) region (decreasing V_1 and increasing V_2). We express the detuning $\epsilon(t)$ in millivolts along V_2 and define the initial detuning as dV_2 relative to the middle of the (1,1,1) region, i.e., halfway between ϵ_- and ϵ_+.

Figure 1(b) also shows features below the (2,0,1)/(1,1,1) charge-transfer line that correspond to coherent oscillations between the spin states of our linear triple dot.[10] The terminology used here to describe these spin states follows that of Laird *et al.*[9] Based on that formulation, the Hamiltonian for a system of three electron spins in the presence of a magnetic field is as follows:

$$H = J_{LC}\left(\vec{S}_L \cdot \vec{S}_C - \tfrac{1}{4}\right) + J_{RC}\left(\vec{S}_R \cdot \vec{S}_C - \tfrac{1}{4}\right) - E_z\left(S_L^z + S_C^z + S_R^z\right), \quad (1)$$

where J_{ij} is the exchange interaction between spins in dots i and j, $\vec{S}_i$ is the spin in dot i, and E_Z is the Zeeman energy. Effective lever arms $\tilde{\alpha}_{LC}$ and $\tilde{\alpha}_{RC}$ are calculated from capacitance ratios and pulse angles in the V_1-V_2 plane and give the conversion from detuning in gate voltage units of millivolts into energy in μeV. From Ref. 9, the three-spin system is characterized by eight eigenvectors, which are divided into two subgroups by the exchange energy: four quadruplet states Q with a total spin $S = 3/2$ ($S_z = \pm 3/2, \pm 1/2$) and two pairs of doublet states Δ and Δ' with a total spin $S = 1/2$ ($S_z = \pm 1/2$).

Here, we consider the positive S_z subset of states,

$$|Q_{1/2}\rangle = \frac{1}{\sqrt{3}}(|\uparrow\uparrow\downarrow\rangle + |\uparrow\downarrow\uparrow\rangle + |\downarrow\uparrow\uparrow\rangle), \quad (2)$$

$$|\Delta_{1/2}\rangle = \frac{1}{\sqrt{4\Omega^2 + 2\Omega(J_{LC} - 2J_{RC})}}[(J_{LC} - J_{RC} + \Omega)|\uparrow\uparrow\downarrow\rangle + (J_{RC} - \Omega)|\uparrow\downarrow\uparrow\rangle - J_{LC}|\downarrow\uparrow\uparrow\rangle], \quad (3)$$

$$|Q_{3/2}\rangle = |\uparrow\uparrow\uparrow\rangle, \quad (4)$$

$$|\Delta'_{1/2}\rangle = \frac{1}{\sqrt{4\Omega^2 + 2\Omega(2J_{RC} - J_{LC})}}[(-J_{LC} + J_{RC} + \Omega)|\uparrow\uparrow\downarrow\rangle - (J_{RC} + \Omega)|\uparrow\downarrow\uparrow\rangle + J_{LC}|\downarrow\uparrow\uparrow\rangle], \quad (5)$$

where $\Omega = \sqrt{J_{LC}^2 + J_{RC}^2 - J_{LC}J_{RC}}$. These states are plotted in Fig. 1(c) as a function of the V_2 component of the applied pulse, denoted here as $\epsilon(t)$. J_{LC} [J_{RC}] is the exchange energy for the left-center [right-center] dot pair. Figure 1(c) does not include the anticrossings induced by hyperfine nuclear gradients.[11,13,14] In the limits of large $|\epsilon|$, the $\Delta'_{1/2}(\Delta_{1/2})$

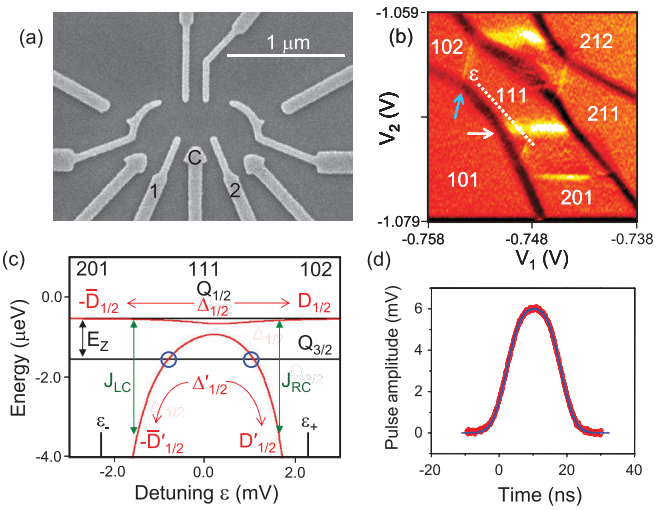

FIG. 1. (Color online) (a) Electron micrograph of the triple dot structure. Fast voltage pulses $(\delta V_1, \delta V_2)$ are applied to gates 1 and 2 in addition to dc voltages (V_1, V_2). Gate C tunes the (1,1,1) region size. (b) Stability diagram obtained from numerically differentiating the left QPC detector conductance with respect to V_2 at $B = 40$ mT. Black is low, red (gray) is medium, and yellow (white) is high. Charge addition lines appear black, and charge-transfer lines appear yellow (white).[7] A typical detuning line is drawn across the (2,0,1)/(1,1,1) charge-transfer line (ϵ_-) indicated by the white arrow and reaches a region close to the (1,0,2)/(1,1,1) charge-transfer line (ϵ_+) indicated by the blue (gray) arrow. (c) Relevant three-spin state energies in the absence of hyperfine coupling as a function of the detuning component along V_2. ϵ_- and ϵ_+ denote the positions of charge-transfer lines along V_2. (d) Calculated (line) and experimental (circles) Gaussian-filtered pulses for pulse duration $\tau = 16$ ns and a rise time of 6.6 ns.

doublet state evolves to the $-\bar{D}'_{1/2}$ $(-\bar{D}_{1/2})$ and $D'_{1/2}$ $(D_{1/2})$ states, respectively, of Ref. 9 on the left and right sides of Fig. 1(c). For example, on the left side of Fig. 1(c), we have

$$|\bar{D}_{1/2}\rangle = \frac{-1}{\sqrt{6}}(2|\uparrow\uparrow\downarrow\rangle - |\uparrow\downarrow\uparrow\rangle - |\downarrow\uparrow\uparrow\rangle), \quad (6)$$

$$|\bar{D}'_{1/2}\rangle = \frac{1}{\sqrt{2}}(|\uparrow\downarrow\uparrow\rangle - |\downarrow\uparrow\uparrow\rangle). \quad (7)$$

The doublet $\Delta'_{1/2}$ state crosses the quadruplet $Q_{3/2}$ state at two places indicated by blue circles in Fig. 1(c). The $Q_{3/2}/Q_{1/2}$ spacing is the Zeeman energy E_z. The $\Delta'_{1/2}/Q_{3/2}$ crossings occur at detunings that vary with magnetic field and map out the "spin arch" used to characterize the system for modeling purposes.[10] The arch is shown as a dashed line in Figs. 2 and 3. The presence of x, y components of hyperfine field gradients between the dots causes the $\Delta'_{1/2}/Q_{3/2}$ crossings to become anticrossings.[14] Likewise, z components of hyperfine gradients lead to additional couplings with the $Q_{1/2}$ state near the maximum of the spin arch. In this device, we find hyperfine couplings around 0.1–0.2 μeV.

For these experiments, a rectangular voltage pulse of duration τ (fixed at 16 ns) and amplitude $(\delta V_1, \delta V_2) = (-5.4, 6.0)$ mV is filtered with a rise time of 6.6 ns as shown in Fig. 1(d). Standard spin-to-charge conversion is used in the (2,0,1) region (where the pulse starts and ends) during spin projection measurements to obtain the doublet

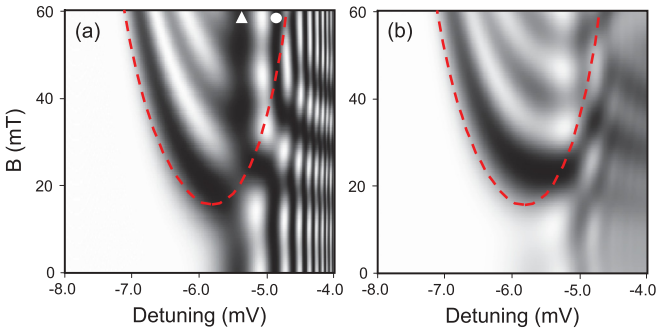

FIG. 2. (Color online) (a) Theoretical map of $P_{\bar{D}'_{1/2}}$ as a function of initial detuning dV_2 and magnetic field B. Black (white) is low (high). $\epsilon_+ - \epsilon_- = 4.6$ mV along V_2. The dashed line is the spin arch. No z-hyperfine couplings are included. Triangle marks first exchange fringe corresponding to π rotation around the $\bar{D}'_{1/2}/\bar{D}_{1/2}$ Bloch sphere x axis. Circle indicates conditions for Bloch sphere calculations in Fig. 4. (b) Same as (a) but including z-hyperfine couplings and charge noise.

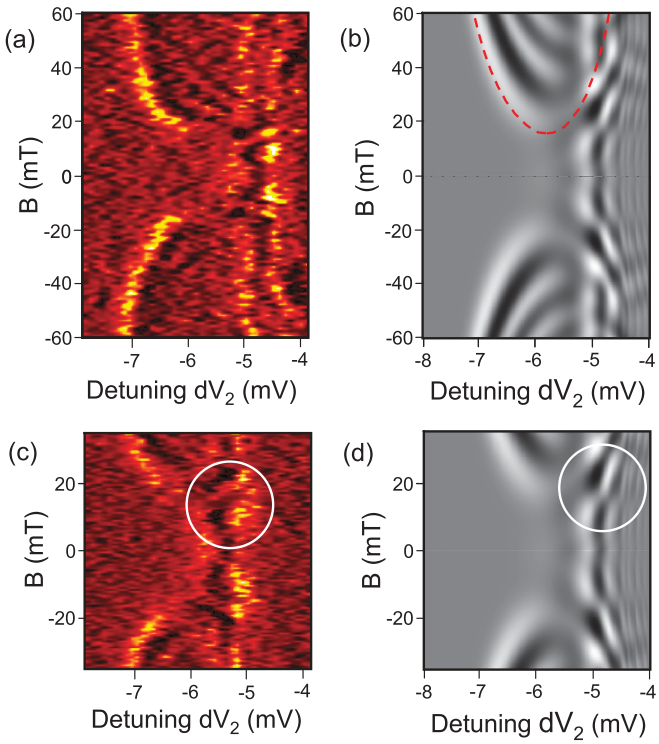

FIG. 3. (Color online) (a) and (c) Experimental derivative of the left QPC conductance with respect to initial detuning dV_2 along V_2 as a function of dV_2 and magnetic field B for a 16-ns rectangular pulse Gaussian filtered with a 6.6-ns rise time and amplitude $(\delta V_1, \delta V_2) = (-5.4, 6.0)$ mV to traverse the charge-transfer line between (2,0,1) and (1,1,1). Black is low, orange (gray) is medium, and yellow (white) is high transconductance. (b) and (d) Calculated derivative with respect to detuning of probability $P_{\bar{D}'_{1/2}}$. Black is low, white is high. $\epsilon_+ - \epsilon_- = 4.6$ mV along V_2. The dashed line in (b) is the experimentally extracted spin arch obtained from the $\Delta'_{1/2}/Q_{3/2}$ crossings illustrated with circles in Fig. 1(c) and underpins the calculations.

occupation probability $P_{\bar{D}'_{1/2}}$.[15] Applying a detuning pulse across a $\Delta'_{1/2}/Q_{3/2}$ anticrossing will result in a phase accumulation between the quantum state components. This phase is related both to the pulse duration and to the detuning voltage.[10,11,16–20]

The spin state evolution in response to the pulse is calculated from the time dependence $d\rho/dt = i[\rho, H/\hbar]$ of the density matrix ρ in the $Q_{1/2}/\bar{D}_{1/2}/Q_{3/2}/\bar{D}'_{1/2}$ basis[10] starting from an initial state at large negative detuning where $P_{\bar{D}'_{1/2}} = 1$. This yields four differential equations solved using the Runge-Kutta method.

In Fig. 2, we show calculated maps of the probability $P_{\bar{D}'_{1/2}}$ of the system returning after the pulse in state $P_{\bar{D}'_{1/2}}$ as a function of initial detuning component dV_2 along V_2 and magnetic field B. Figure 2(a) shows the case where we have included the $\Delta'_{1/2}/Q_{3/2}$ (xy)-hyperfine coupling but not the z-hyperfine coupling that would play a role when the exchange splitting is small. Multiple oscillations due to the spin arch anticrossings are clearly seen. These features correspond to a special case of the tripartite qubit model of Sun *et al.* describing interference effects observed due to a state anticrossing with two other states.[21] In our case, the two states are replaced by a dispersing state $(\Delta'_{1/2})$ that crosses a dispersionless state $(Q_{3/2})$ twice. Interfering with these magnetic-field-dependent oscillations defined by the $\Delta'_{1/2}/Q_{3/2}$ energy splitting are magnetic-field-independent oscillations defined by the exchange interaction (vertical fringes appearing at initial detunings > -6.0 mV). The first of these, at around -5.4 mV (marked with a triangle), corresponds to a π rotation around the x axis on the $\bar{D}'_{1/2}/\bar{D}_{1/2}$ Bloch sphere. Starting at around -4.9 mV, we see a series of fringes associated with exchange coupling on the right-hand side of Fig. 1(c) where J_{RC} is increasing. Due to the strength of the exchange fringes, any interference between the first and the second $\Delta'_{1/2}/Q_{3/2}$ beam splitters is masked. Instead, we see additional diagonal fringes to the right of the figure, corresponding to interference between the $\Delta'_{1/2}/Q_{3/2}$ and the exchange interactions. In Fig. 2(b), we now include z-hyperfine couplings between the $\Delta'_{1/2}/Q_{1/2}$ and the $Q_{1/2}/\Delta_{1/2}$ states. Due to z-hyperfine enhancement during the pulse,[10] we take the z coupling to be twice the xy coupling. This causes the first exchange fringe near the minimum exchange splitting to almost disappear but has less impact for fringes to the right of this point. Hyperfine averaging leads to slight additional blurring of the exchange fringes. We average over a small range (about 0.4 mV) of detuning to model charge noise effects.

In Fig. 3(a), we show an experimental map of the numerical derivative of the left QPC conductance with respect to initial detuning component dV_2 as a function of dV_2 and the magnetic field. The spin arch is observed for both signs of the magnetic field. Figure 3(a) shows another experiment focused slightly to emphasize an interesting region corresponding to the maximum amplitude of the pulse reaching the right-side anticrossing. The dominant feature is a pair of B-independent vertical fringes around an initial detuning of -5.0 mV. These are due to exchange oscillations and are observed without recourse to initialization under the z-hyperfine field as in the paper of Petta *et al.*[13] In addition, these fringes are crossed by B-dependent fringes corresponding to the beam

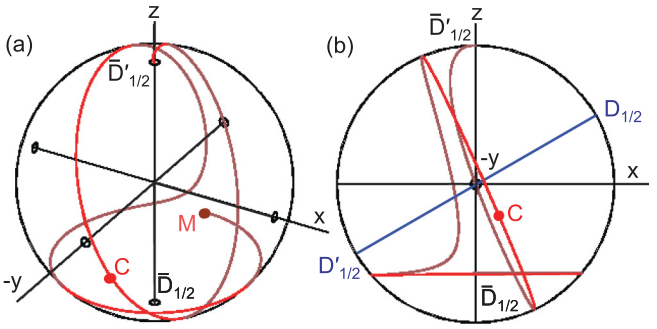

FIG. 4. (Color online) (a) and (b) Two views of the $\bar{D}'_{1/2}/\bar{D}_{1/2}$ Bloch sphere showing same calculated state vector motion during the pulse at the point in Fig. 2(a) marked by a circle [(b) shows the projection on the xz plane]. Point C marks the peak of the pulse, and point M marks where the pulse has returned to the (2,0,1) measurement region.

splitter oscillations. These are highlighted with a circle. The experimental resolution vanishes very quickly in this region of rapid oscillation, probably due to charge noise effects as in Fig. 2(b). For comparison, the equivalent theoretical derivatives of $P_{\bar{D}'_{1/2}}$ from Fig. 2(b) are plotted in Figs. 3(b) and 3(d). We assume that T_2^* is infinite here, but a value of 10 ns, consistent with previous analysis,[10,22] slightly reduces the contrast. The far- (right-) side beam splitter modulation of the exchange oscillations in the experiment corresponds to the features highlighted by the circle in Fig. 3(d). This is analogous to an interplay described for the double dot regime[22] but corresponds here to spin operations on the far (RC) side of the dot from the (2,0,1) measurement region.

To confirm the nature of the B-independent fringes, in Figs. 4(a) and 4(b), we plot two views of the $\bar{D}'_{1/2}/\bar{D}_{1/2}$ Bloch sphere with the motion of the state vector as a function of pulse time for the detuning/field point marked with a circle in Fig. 2(a). This fringe is due to J_{RC} exchange rotation on the right side of Fig. 1(c). The trajectory lies on the sphere surface since the radial position is normalized to unity from the sum of the $\bar{D}'_{1/2}$ and $\bar{D}_{1/2}$ diagonal elements in the density matrix and we have neglected dephasing in this plot. This basis for this particular Bloch sphere corresponds to the (2,0,1) (LC) side of the triple dot system where the pulse starts and ends, and in Fig. 4(b), we have added the axis corresponding to the $D'_{1/2}/D_{1/2}$ states on the far (RC) side. At the peak of the pulse (C), the state vector rotates around this axis before returning to rotate around the polar axis for measurement (we have terminated the trajectory early). A similar plot (not shown) for the second vertical fringe has an additional rotation around the $D'_{1/2}/D_{1/2}$ axis.

In conclusion, we have studied the coherent behavior of three interacting spins in a triple quantum dot as the system evolves through the anticrossings on both sides of the energy-level diagram. In our experimental and theoretical results, we find that double beam splitter behavior, driven by the hyperfine interaction (LZS), interplays with the pure exchange oscillations proposed by DiVincenzo *et al.* as encoded qubits.[1]

We acknowledge W. A. Coish, L. Gaudreau, M. Pioro-Ladrière, A. Clerk, D. G. Austing, and R. Brunner for discussions, and O. Kodra for programming. A.S.S. acknowledges funding from NSERC and CIFAR. G.G. acknowledges funding from the NRC-CNRS Collaboration and CIFAR.

*andrew.sachrajda@nrc.ca

[1] D. P. DiVincenzo, D. Bacon, J. Kempe, G. Burkard, and K. B. Whaley, Nature (London) **408**, 339 (2000).
[2] A. D. Greentree, J. H. Cole, A. R. Hamilton, and L. C. L. Hollenberg, Phys. Rev. B **70**, 235317 (2004).
[3] B. Michaelis, C. Emary, and C. W. J. Beenakker, Europhys. Lett. **73**, 677 (2006).
[4] M. Busl, R. Sanchez, and G. Platero, Phys. Rev. B **81**, 121306(R) (2010).
[5] P. Hawrylak and M. Korkusinski, Solid State Commun. **136**, 508 (2005).
[6] L. Gaudreau,, A. Kam, G. Granger, S. A. Studenikin, P. Zawadzki, and A. S. Sachrajda, Appl. Phys. Lett. **95**, 193101 (2009).
[7] G. Granger, L. Gaudreau, A. Kam, M. Pioro-Ladrière, S. A. Studenikin, Z. R. Wasilewski, P. Zawadzki, and A. S. Sachrajda, Phys. Rev. B **82**, 075304 (2010).
[8] D. Schroer, A. D. Greentree, L. Gaudreau, K. Eberl, L. C. L. Hollenberg, J. P. Kotthaus, and S. Ludwig, Phys. Rev. B **76**, 075306 (2007).
[9] E. A. Laird, J. M. Taylor, D. P. DiVincenzo, C. M. Marcus, M. P. Hanson, and A. C. Gossard, Phys. Rev. B **82**, 075403 (2010).
[10] L. Gaudreau, G. Granger, A. Kam, G. C. Aers, S. A. Studenikin, P. Zawadzki, M. Pioro-Ladrière, Z. R. Wasilewski, and A. S. Sachrajda, Nat. Phys. **8**, 54 (2012).
[11] J. R. Petta, H. Lu, and A. C. Gossard, Science **327**, 669 (2010).
[12] M. Field, C. G. Smith, M. Pepper, D. A. Ritchie, J. E. F. Frost, G. A. C. Jones, and D. G. Hasko, Phys. Rev. Lett. **70**, 1311 (1993).
[13] J. R. Petta, A. C. Johnson, J. M. Taylor, E. A. Laird, A. Yacoby, M. D. Lukin, C. M. Marcus, M. P. Hanson, and A. C. Gossard, Science **309**, 2180 (2005).
[14] J. M. Taylor, J. R. Petta, A. C. Johnson, A. Yacoby, C. M. Marcus, and M. D. Lukin, Phys. Rev. B **76**, 035315 (2007).
[15] K. Ono, D. G. Austing, Y. Tokura, and S. Tarucha, Science **297**, 1313 (2002).
[16] C. Zener, Proc. R. Soc. London, Ser. A **137**, 696 (1932).
[17] H. Ribeiro and G. Burkard, Phys. Rev. Lett. **102**, 216802 (2009).
[18] H. Ribeiro, J. R. Petta, and G. Burkard, Phys. Rev. B **82**, 115445 (2010).
[19] J. Särkkä and A. Harju, New J. Phys. **13**, 043010 (2011).
[20] S. Shevchenko, S. Ashhab, and F. Nori, Phys. Rep. **492**, 1 (2010).
[21] G. Sun, X. Wen, B. Mao, J. Chen, Y. Yu, P. Wu, and S. Han, Nature Commun. **1**, 51 (2010).
[22] S. A. Studenikin, G. C. Aers, G. Granger, L. Gaudreau, A. Kam, P. Zawadzki, Z. R. Wasilewski, and A. S. Sachrajda, Phys. Rev. Lett. **108**, 226802 (2012).